

Frictional Duality Observed during Nanoparticle Sliding

Dirk Dietzel,^{1,2} Claudia Ritter,³ Tristan Mönninghoff,¹ Harald Fuchs,^{1,2}

André Schirmeisen,¹ and Udo D. Schwarz³

¹*Institute of Physics and Center for Nanotechnology (CenTech), University of Münster,*

Münster, Germany

²*INT, Forschungszentrum Karlsruhe (FZK), Karlsruhe, Germany*

³*Department of Mechanical Engineering and Center for Research on Interface*

Structures and Phenomena (CRISP), Yale University, New Haven, CT, USA.

PACS number(s): 07.79.Sp, 46.55.+d, 81.40.Pq, 62.20.Qp

One of the most fundamental questions in tribology concerns the area dependence of friction at the nanoscale. Here, experiments are presented where the frictional resistance of nanoparticles featuring particle-substrate contact areas of 8,000-310,000 nm² is measured by pushing them with the tip of an atomic force microscope. We find two coexisting frictional states: While some particles show finite friction increasing linearly with interface area, other particles assume a state of frictionless sliding. Analysis suggests the degree of surface contamination being decisive for this duality.

In recent years, considerable efforts have been directed towards the clarification of the atomic origins of friction [1], largely spurred by the ongoing miniaturization of moving components in technological devices and the advent of new techniques allowing nanometer-scale tailoring of tribological surface coatings [2]. One of the most debated subjects in this context is how the frictional force F_f experienced at a finite, atomically flat interface of nanoscopic dimensions scales with the actual contact area A . Macroscopically, Amontons' well-known law $F_f = \mu F_1$ applies, where F_1 represents the external loading force and μ the friction coefficient. Since μ is constant for a given material combination, friction is independent of the dimensions of the interface. If, however, we perform the transition from the *apparent* macroscopic contact area to the *true dimensions* of the nanometre-sized single asperity contacts that actually support the macroscopic sliders, this behaviour changes.

So far, only two studies using realistically sized isolated nanocontacts, which can be as large as some $100,000 \text{ nm}^2$, have been published, both indicating linear dependencies between friction and contact area [3,4]. Their interpretation, however, is hampered because they have not been performed under well-defined vacuum conditions. In contrast, other reports indicate that virtually frictionless sliding may exist under certain conditions for model contacts of only a few nm^2 in size [5-8]. Indeed, for sliding contacts featuring clean, atomically flat, but incommensurate interfaces, theory predicts ‘superlubric’ sliding, as the structural mismatch induces a decrease of the barriers between local minima of the interaction potential with increasing contact size that ultimately leads to vanishing friction [9-12]. This mechanism, which has also been denoted as ‘structural lubricity’ [9] to highlight its atomic-scale origin, is widely held responsible for the excellent lubrication properties of solid lubricants such as graphite

[7] or molybdenum disulfide [13]. The prospect of establishing an analogue regime with sliders used in micromachines motivates our analysis of the frictional properties of *extended* nanocontacts with varying size under controlled conditions.

The present lack of knowledge in this regard stems from the fact that established experimental procedures are severely limited due to a size gap between the small contact areas of scanning probe microscopes (few nm²) [5-8] and the contact areas offered by the surface force apparatus (some ten thousands of μm²) [14,15]. To overcome this gap, we performed experiments where the frictional resistance of nanoparticles is measured while they are pushed by the tip of an AFM. Nanoparticle manipulation has been rarely used for quantitative, statistically significant friction studies so far [3,4]. Fig. 1(a) illustrates how particle translation has been realized in the present work; the applied data acquisition and analysis procedures have been developed specifically for this investigation and are presented in detail elsewhere [16]. Basically, quantitative values for the particle's frictional resistance are extracted from individual line traces of the friction signal acquired during manipulation (Fig. 2).

As sample, we chose antimony grown on highly oriented pyrolytic graphite (HOPG) (see Fig. 1(b)). This material combination has not only been proven to be well suited for manipulation experiments under ambient conditions [4], but its growth and structure have also been characterized earlier [17]. If not stated otherwise, HOPG substrates were cleaved under ambient conditions, immediately introduced into the vacuum chamber ($p < 5 \times 10^{-10}$ mbar) and subsequently heated in-situ to ≈ 150 °C for 1 h in order to ensure clean surface conditions. Antimony was evaporated from the solid phase at 370°C for 20 minutes. A low evaporation rate was chosen, which resulted in

mostly round or only modestly ramified islands of 50-750 nm in diameter and up to 80 nm in height ideally suited for translation experiments. All four independent data sets presented have been obtained at room temperature. For data sets #1 and #2, experiments were carried out using Omicron Nanotechnology's standard ultrahigh vacuum (UHV) AFM system, while set #3 was recorded using their VT-series UHV-AFM. In both cases, the sample was transferred from the preparation stage to the AFM without breaking the vacuum. Complementary experiments were executed under ambient conditions using a Veeco Multimode AFM (set #4).

Data sets #1 and #2 represent an original experiment (circular markers in Figs. 3(a) and (b)) and a control experiment (square markers) that have been performed with two different cantilevers and different, but identically prepared samples. The results of 31 dislocation events using particles featuring contact areas between 22,000 nm² and 90,000 nm² are presented in Fig. 3(a). These events can be categorized in two distinct regimes: While the majority featured substantial frictional resistance (regime 1; black symbols), about 1/4 of the events showed almost no detectable friction (regime 2; red symbols), causing an apparent 'frictional duality'.

To clarify the friction-size relation for the events with substantial frictional resistance, we extended the experiments by including particles up to $A = 310,000 \text{ nm}^2$. The results shown in Fig. 3(b) suggest a linear dependence and a constant shear stress $\tau = F_l/A = (1.04 \pm 0.06) \text{ MPa}$. Since the normal force experienced by the particles is due to adhesion, which scales linearly with area, an area-independent friction coefficient follows, reinforcing Amontons' law also at the nanoscale. Note that τ is almost identical to values found for Cd arachidate islands ($\approx 1 \text{ MPa}$) [18] and MoO₃ nanocrystals

(≈ 1.1 MPa) [3] moved at ambient pressure, but roughly one order of magnitude higher than for C_{60} islands displaced on NaCl in UHV [19].

To discuss the observed coexistence of two frictional states, let us consider four different scenarios: (i) Particles showing no apparent friction are picked up by the tip during translation. (ii) Particles showing no apparent friction are stuck on a graphite flake, which slides superlubric [7]. (iii) Particles are crystalline and exhibit well-ordered, crystalline interfaces. Depending on the particle lattice's orientation relative to the substrate, finite friction (commensurate) or vanishing friction (incommensurate) will be observed [5,7,12]. (iv) While clean interfaces may exhibit superlubric behavior due to structural mismatch (particles may be crystalline or amorphous), mobile molecules (such as hydrocarbon or water molecules) trapped between the sliding surfaces cause a breakdown of the superlubric behavior [9,20]. Often referred to as 'dirt particles', these molecules are able to move to positions where they simultaneously match the geometry of both top and bottom surfaces, thus augmenting the height of the bottom surface in a way that matches the (atomic-scale) undulations of the top surface [9]. As a consequence, an area independent friction coefficient is obtained.

From these scenarios, (i) can be discarded as frictionless displaced particles are imaged after translation if they get stuck at an obstacle in their way (see e.g. Fig. 4). Also, it seems energetically not feasible for a tip to lift a plate-like particle off the surface that is adhesively bond to the surface by an area much larger than any of its side faces. Next, we consider (ii) being unlikely for three reasons: (1) "after"-images show no sign of missing graphite flakes, (2) the creation of a graphite flake of the size of a nanoparticle by rupturing it off a larger graphite layer would require the breaking of

thousands of covalent carbon-carbon bonds and thus include a very high energetic penalty, and (3) as presented later, the two initially superlubric manipulation events observed at ambient conditions turned into “regular” events featuring finite friction after a short travel distance, which would be difficult to understand in this picture.

To discuss (iii), we note that it requires the presence of a commensurate crystalline interface, while the compact shape of the particles used for sets #1 and #2 suggests them being amorphous [17]. In either case, the atomic lattices of Sb and HOPG do not match, i.e., the interfaces are incommensurate and superlubric behavior should prevail, even though the existence of Moire-type potential minima for certain relative lattice orientations may be conceivable. In any case, if we assume (iii) being correct, it would still be surprising that the superlubric state only occurs for $\approx 1/4$ of the investigated islands, while most particles still exhibit ‘Amontons-like’ sliding. Furthermore, if we translate particles that exhibit friction multiple times (up to 22 subsequent manipulations have been performed with the same particle), no statistically relevant change of the observed frictional force is observed [16], even though a small rotation of the particle would already lead to incommensurate conditions inducing vanishing friction. These arguments make scenario (iii) appear rather unlikely.

Scenario (iv) finally assumes adsorbed but mobile molecules that are trapped between the sliding surfaces. This is likely to happen, as even “clean” UHV conditions are insufficient to avoid the presence of adsorbates over long periods of time (sets #1 & #2 were collected over several weeks). Further, the HOPG samples for these data sets have been cleaved in ambient conditions, and the subsequent in-situ cleaning by heating might have been insufficient. Therefore, we improved the experimental procedure by

cleaving the HOPG crystal *inside* the UHV chamber and conducting all experiments within two days while focusing on smaller islands ($<40,000 \text{ nm}^2$). As a consequence, the ratio of particles showing no friction was greatly increased to over one half of the manipulated particles in the corresponding set #3 (triangles in Fig. 3(a)).

In addition, the opposite case of very contaminated surfaces was investigated in a fourth experimental series performed under ambient conditions (Fig. 3(c)). Friction now increased by a factor of 40, and the vast majority of islands now exhibited ‘Amontons-like’ sliding as found earlier [4]. A parallel analysis of the particles by cross-sectional transmission electron microscopy revealed that the exposure to air converts the particle’s surfaces to amorphous antimony oxide, disregarding whether a particle has originally been amorphous or crystalline. While this structural transition might at least partially explain the huge change in frictional resistance, it also implies that all particles should slide frictionless due to structural mismatch assuming the validity of scenario (iii), which is clearly not the case. Nevertheless, we found two events, recorded shortly (hours) after exposing the sample to air that exhibited vanishing friction. Interestingly, both particles involved into these events translated only less than 100 nm superlubric, then converting into “regular” particles exhibiting substantial friction upon subsequent manipulation.

Summarizing our above discussion, only scenario (iv) remains without apparent contradictions. Further, we could successfully link the ratio of superlubric to non-superlubric events to sample cleanliness and observed the transition from superlubric to “regular” sliding for particles translated in air. On the other hand, it seems surprising that the experienced finite friction is very reproducible in all experiments. Intuitively,

one would expect a certain variation with degree of contamination especially for the low-contamination experiment (data set #3), even though simulations see very little influence of the level of contamination on friction for a coverage between one quarter and a full monolayer [20]. Also, these predictions might need to be modified for the present case of a pure adhesive load. In any case the ambient manipulation experiments prove that the superlubric state can, if only rarely and for short distances, be observed even under strongly contaminated conditions, which gives hope for future technical applications of frictionless sliding. Certainly, it will be a challenge for scientists and engineers to find routes that translate these findings into practical realization with micromachines.

The authors thank Lars Jansen (University of Münster) for technical support, Hendrik Hölscher (University of Münster), Markus Heyde (Fritz-Haber-Institute, Berlin), and Martin Müser (University of Western Ontario, London) for discussions. Work at Münster was supported by the Deutsche Forschungsgemeinschaft and the FANAS Initiative of the European Science Foundation, work at Yale by the Petroleum Research Fund of the American Chemical Society (grant No.\ PRF 42259-AC5) and the National Science Foundation (grant No.\ MRSEC DMR 0520495). C. R. acknowledges the receipt of a personal stipend by the Deutsche Forschungsgemeinschaft.

References

- [1] E. Gnecco and E. Meyer (Eds.) Fundamentals of Friction and Wear on the Nanoscale (Springer, Berlin, Germany, 2007).
- [2] Bhushan, B. (Ed.) Nanotribology and Nanomechanics (Springer, Berlin, Germany, 2005).
- [3] P.E. Sheehan and C.M. Lieber, Science **272**, 1158 (1996).
- [4] C. Ritter, M. Heyde, B. Stegemann, K. Rademann and U.D. Schwarz, Phys. Rev. B **71**, 085405 (2005).
- [5] M. Hirano, K. Shinjo, R. Kaneko and Y. Murata, Phys. Rev. Lett. **78**, 1448 (1997).
- [6] A. Crossley, E.H. Kisi, J.W.B. Summers and S. Myhra, J. Phys. D **32**, 632 (1999).
- [7] M. Dienwiebel, G.S. Verhoeven, N. Pradeep, J.W.M. Frenken, J.A. Heimberg and H.W. Zandbergen, Phys. Rev. Lett. **92**, 126101 (2004).
- [8] A. Socoliuc, R. Bennewitz, E. Gnecco and E. Meyer, Phys. Rev. Lett. **92**, 134301 (2004).
- [9] M.H. Müser, L. Wenning and M.O. Robbins, Phys. Rev. Lett. **86**, 1295 (2001).
- [10] M.H. Müser, Europhys. Lett. **66**, 97 (2004).
- [11] M. Hirano and K. Shinjo, Phys. Rev. B **41**, 11837 (1990).
- [12] K. Shinjo and M. Hirano, Surf. Sci. **283**, 473 (1993).
- [13] J.M. Martin, C. Donnet, T.L. Mogne and T. Epicier, Phys. Rev. B **48**, 10583 (1993).
- [14] J.N. Israelachvili, J. Colloid Interface Sci. **44**, 259 (1973).
- [15] A.M. Homola, J.N. Israelachvili, P.M. McGuiggan and M.L. Gee, Wear **136**, 65 (1990).

- [16] D. Dietzel, T. Mönninghoff, L. Jansen, H. Fuchs, C. Ritter, U.D. Schwarz and A. Schirmeisen, J. Appl. Phys. **102**, 084306 (2007).
- [17] B. Stegemann, C. Ritter, B. Kaiser and K. Rademann, J. Phys. Chem. B **108**, 14292 (2004).
- [18] E. Meyer, R. Overney, D. Brodbeck, L. Howald, R. Lüthi, J. Frommer and H.-J. Güntherodt, Phys. Rev. Lett. **69**, 1777 (1992).
- [19] R. Lüthi, E. Meyer, H. Haefke, L. Howald, W. Gutmannsbauer, H.-J. Güntherodt, Science **266**, 1979 (1994).
- [20] G. He, M.H. Müser and M.O. Robbins, Science **284**, 1650 (1999).

Figures

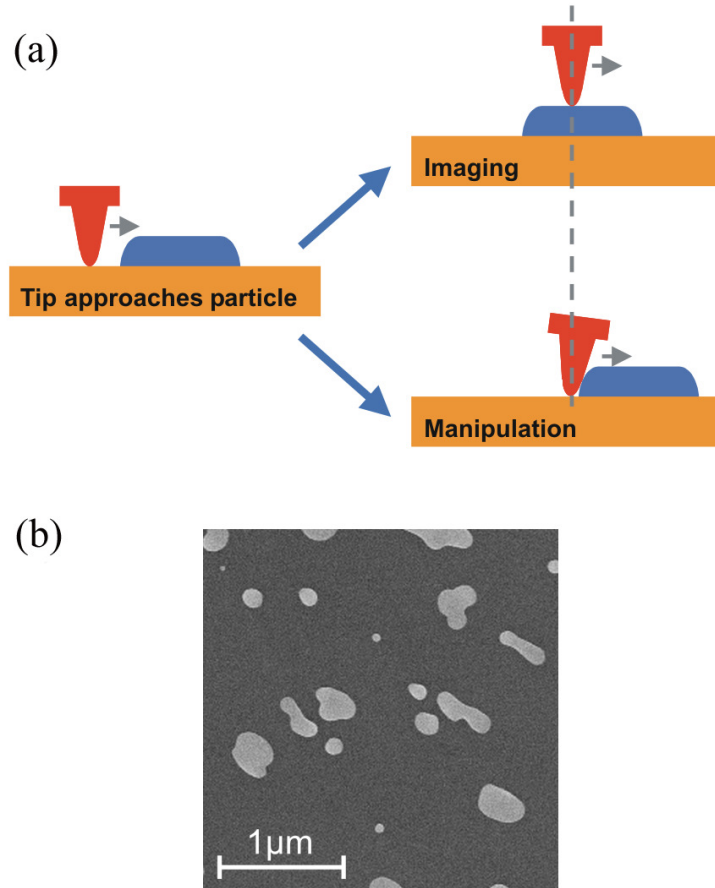


FIG. 1. (a) Scheme of particle manipulation experiments. *Imaging*: Below a certain normal threshold force, the cantilever traces the topography accurately without moving the nanoparticle. *Manipulation*: At loads larger than manipulation threshold, the tip pushes the particle out of its way. In this case, an additional lateral force manifesting as enhanced cantilever torsion can be observed, which corresponds to the particle's frictional resistance. (b) Scanning electron micrograph of one of the samples (Sb islands on HOPG) used for the translation experiments.

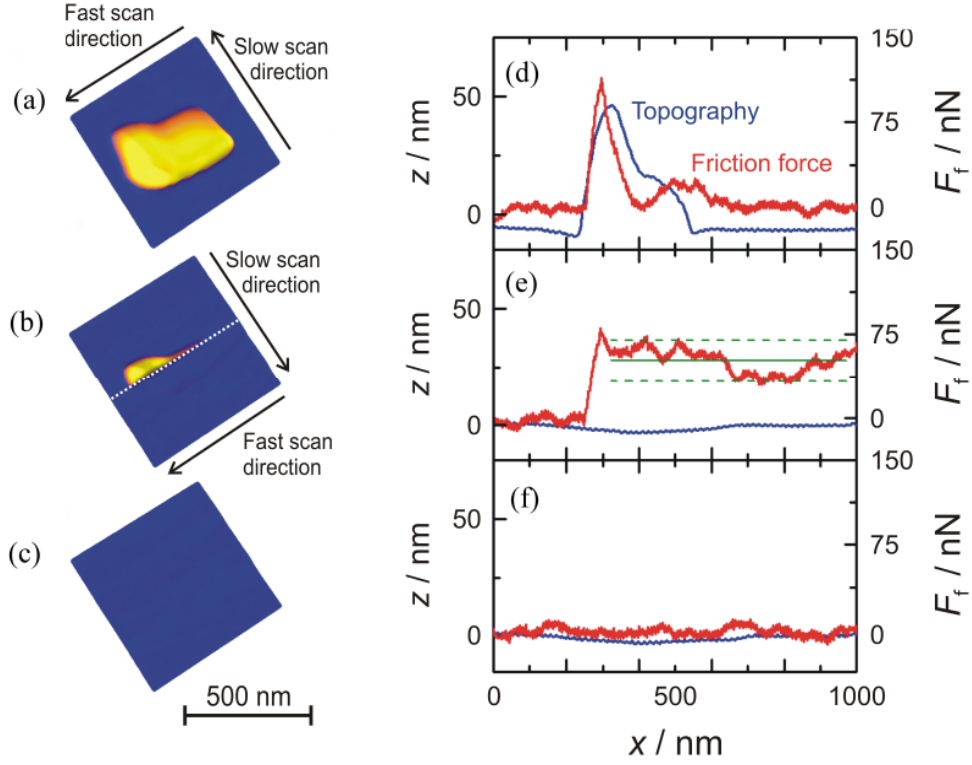


FIG. 2. Illustration of the manipulation procedure. (a) A nanoparticle is imaged for accurate contact area determination at low external loading force to prevent displacement. (b) The load is increased slightly above the manipulation threshold. Since the force necessary to initiate particle motion for the first time is typically higher than in subsequent manipulation events, the particle is imaged for several line scans before it is pushed out of the field of view (along white dotted scan line), which results in the appearance of a “cut” particle. (c) Subsequent imaging with low loads confirms successful particle translation. (d) Line scans representing the topography (blue, left axis) and the simultaneously recorded lateral force (green, right axis) of the last scan line before translation. The lateral force signal is mainly topography-induced, as the cantilever twists at the particle’s edges. (e) Scan line during which the displacement occurred (white dotted line in b). The topographic signal now reflects the surface of the

bare graphite, while the average frictional resistance of the particle (≈ 260 nN, solid red line) and its standard deviation (dashed red lines) can be determined from the lateral force signal. (f) First scan line following the manipulation event proving that the particle has been removed.

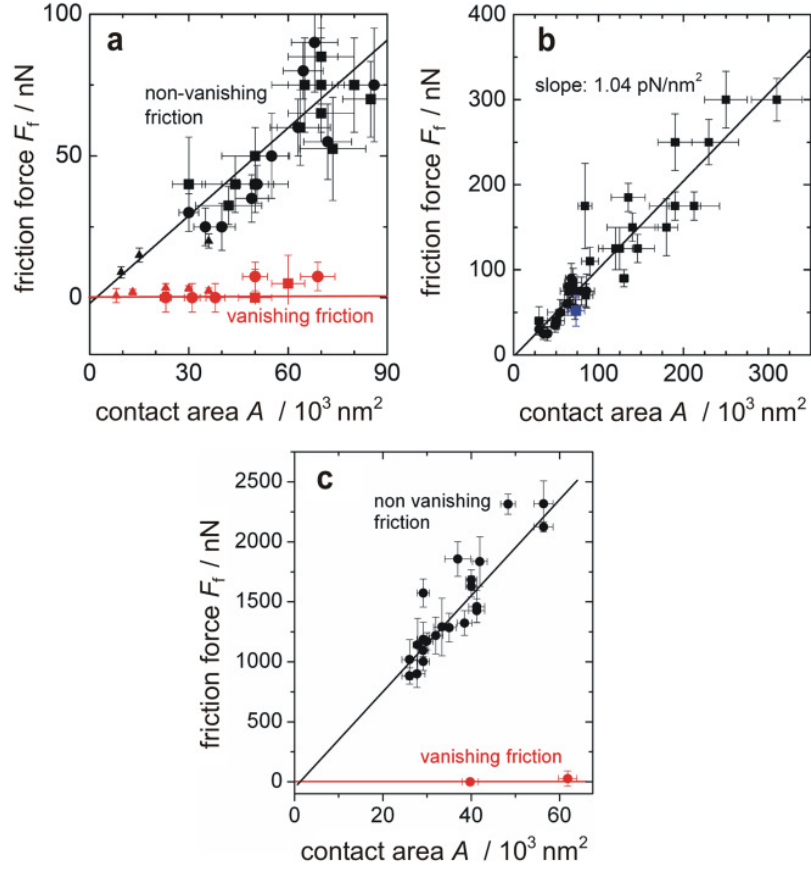


FIG. 3. (a) Data obtained under UHV conditions, uncovering two distinct frictional regimes for particle/sample contact areas up to $90,000 \text{ nm}^2$. Regime 1 (black-colored symbols) comprises particles with substantial friction whereas particles that exhibit virtually no measurable friction (red-colored symbols) are assigned to regime 2. The square marker and circular markers represent measurements for two similar prepared samples with different cantilevers. Triangular markers show a third set of measurements with focus on smaller islands using an alternative UHV-AFM set-up and improved sample preparation (see text for details). (b) Graph featuring 39 non-vanishing friction events under UHV conditions for particle sizes up to $310,000 \text{ nm}^2$. The blue marker highlights the data point derived from Fig. 2(e). The data is well approximated by a

linear fit with $F_f = (1.04 \pm 0.06) \text{ pN/nm}^2 \times A - (2.72 \pm 7.04) \text{ nN}$ (black solid lines in a and b) with no statistically significant offset. (c) Experimental data obtained under ambient conditions for particles with contact areas between 21,000 nm² and 62,000 nm². Two different regimes can once again be identified. The events featuring substantial friction follow an approximate linear dependency with $F_f = (40 \pm 1) \text{ pN/nm}^2 \times A - (48 \pm 74) \text{ nN}$ (black solid line in c).

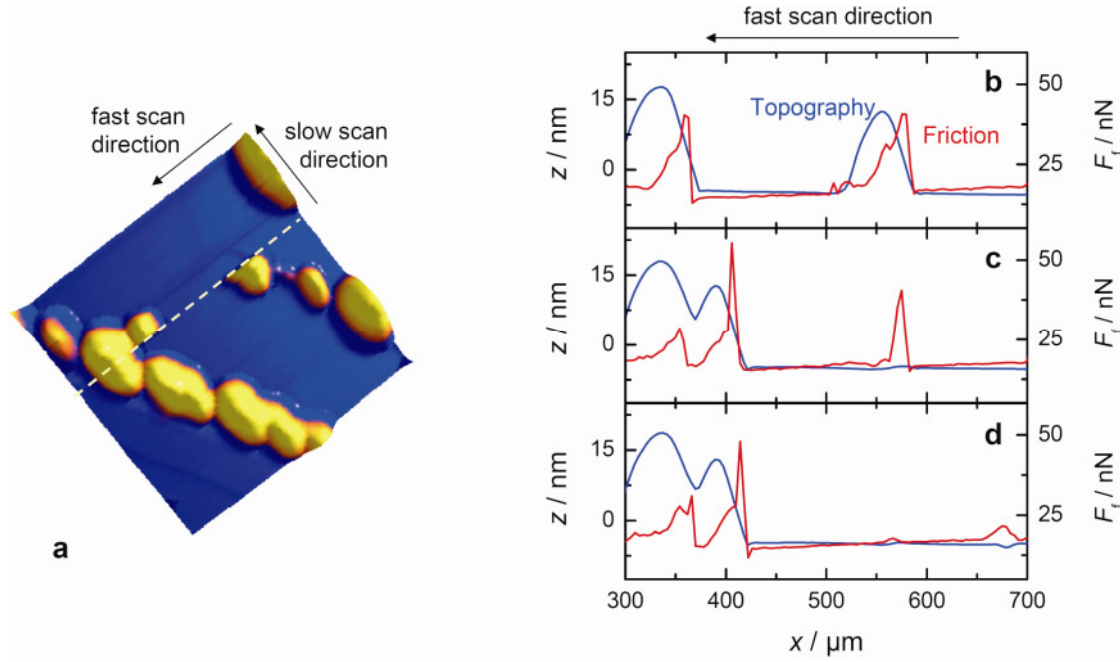


FIG. 4. (a) Topographical scan during which a translation event of an Sb nanoparticle with a contact area of $8,000 \text{ nm}^2$ took place. The particle was displaced during the recording of one single scan line (dashed line) and thus appears “cut”. (b)–(d) The corresponding scan lines just before (b), during (c), and right after (d) the translation of the particle. In contrast to Fig. 2(e), the friction signal here only shows a peak where the tip hits the island at its initial position ($x = 580 \text{ nm}$) and remains flat afterwards until the island reaches its new resting position at $x = 425 \text{ nm}$. The frictional force during translation was well below 1 nN .